

Supporting Information

Additive Electron Pathway and Non-additive Molecular Conductance by Using a Multipodal Bridging Compound

Manabu Kiguchi,^{†*} Yuuta Takahashi,[†] Shintaro Fujii,[†] Masayoshi Takase,[‡] Masahiko Iyoda,^{‡*}

Masayo Horikawa,[§] Yasuhisa Naitoh,[§] and Hisao Nakamura^{§*}

Department of Chemistry, Graduate School of Science and Engineering, Tokyo Institute of
Technology 2-12-1 W4-10 Ookayama, Meguro-ku, Tokyo 152-8551, Japan, Department of
Chemistry, Graduate School of Science and Engineering, Tokyo Metropolitan University, Hachioji,
Tokyo 192-0397, Japan, Nanosystem Research Institute, National Institute of Advanced Industrial
Science and Technology, Central 2, Umezono 1-1-1, Tsukuba, Ibaraki 305-8568, Japan

AUTHOR EMAIL ADDRESS kiguti@chem.titech.ac.jp, iyoda@tmu.ac.jp,

hs-nakamura@aist.go.jp

Telephone number: 81-3-5734-2071

FAX number: 81-3-5734-2071

* Authors to whom correspondence should be addressed. E-mail addresses: kiguti@chem.titech.ac.jp

[†]Tokyo Institute of Technology. [‡]Tokyo Metropolitan University, [§]Advanced Industrial Science and
Technology

S1. Conductance histograms

We constructed conductance histograms using the procedure developed by Huber *et al.*^{S1} The tunneling background on the low- G side follows a $1/G$ dependence. By fitting the raw datasets (black lines in Figure S1) to the $1/G$ function in the low- G regime ($0.000026G_0$ – $0.00024G_0$ for **4-TEB** and $0.0000129G_0$ – $0.0000354G_0$ for **2-TEB**), we obtained the tunneling background (blue dotted lines in Figure S1). The tunneling background was subtracted from the raw datasets, and the obtained curves are shown as red curves in Figure S1.

The procedures used to determine the conductance values and standard deviations were as follows: (I) we constructed a conductance histogram from 1000 conductance traces (one dataset) and determined the first-peak position of the conductance, (II) we repeated procedure (I) for 21 different datasets, and (III) then we determined the conductance values as the average position of the first peaks for the 21 datasets.

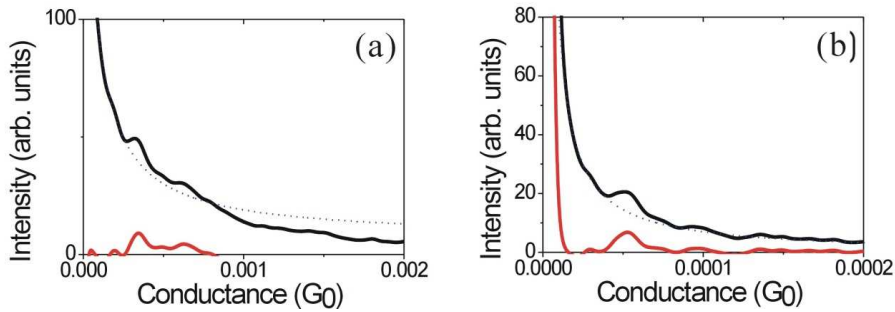


Figure S1. Conductance histograms of Au point contacts broken in tetraglyme solutions containing (a) **4-TEB** and (b) **2-TEB**. The black lines show the raw datasets, and the blue dotted lines show the background, which shows a $1/G$ dependence. The histograms were constructed without data selection from 1000 traces.

Figure S2 display the 2D conductance-versus displacement histograms^{S2} of **2-TEB**, **4-TEB** and blank solution, respectively. We generated the 2D histograms by identifying the first data point in every trace which had the conductance lower than $0.03 G_0$ as a relative zero distance $z = 0$ to overlap all individual traces in 2D space constructed from 2000 conductance traces without data selection.

Compared to the blank solution (Fig. S2c), finite counts were observed for longer stretch length regime for **4-TEB** and **2-TEB** (Fig. S2ab), indicating the formation of the molecular junction. Since the formation probability was low for **2-TEB**, the intensity was low at the average conductance and stretch length regime of the single **2-TEB** molecule junction. Although the count was small, there was local maxim at the average conductance and stretch length regime for both **4-TEB** and **2-TEB**, as shown in Fig. S2ab. The stretch length was longer for **4-TEB** than **2-TEB**. Black circles are guide for eyes. The junction break at the conductance value of ca. $2.5 \times 10^{-4} G_0$ for the histogram of **4-TEB** in FigureS2(a). Conductance distribution at $0.5 \times 10^{-4} G_0$ can be seen for the histogram of **2-TEB** in FigureS2(b).

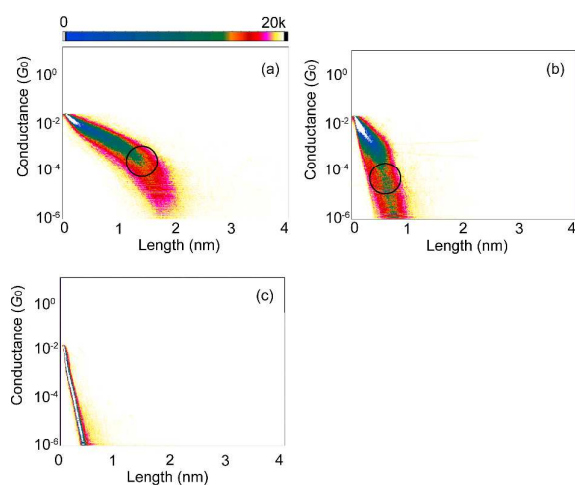


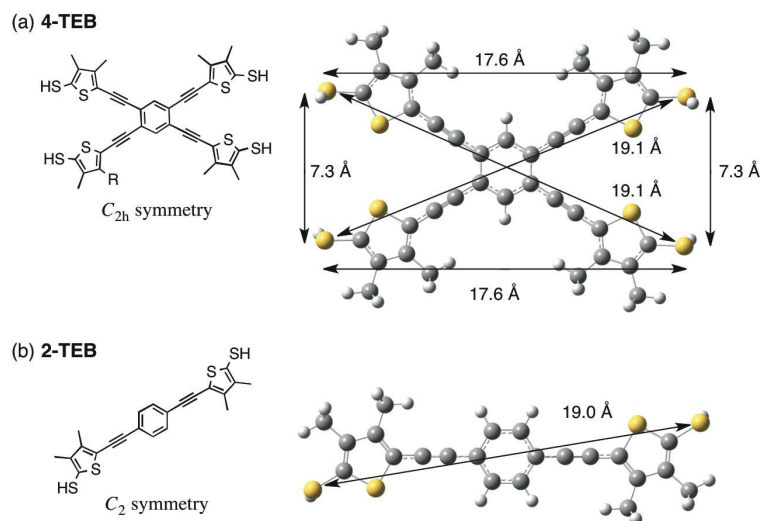
Figure S2. 2D conductance histogram of (a) **4-TEB**, (b) **2-TEB**, (c) blank solution.

S2. Evaluation of plateau length and gap length

To evaluate the molecular sizes of **2-TEB** and **4-TEB**, the optimized structures were determined by using DFT calculations at the B3LYP/6-31G(d) level of theory with simplified models of **2-TEB** (C_2 symmetry) and **4-TEB** (C_{2h} symmetry), where the butyl groups were replaced with methyl groups. Frequency calculations were used to verify that there were no imaginary frequencies in the optimized structures. The structures are shown in Figure S3, together with the distances between the sulfur atoms of the thiol groups. As described in the main text, three possible distances between the sulfur atoms of the thiol groups can be considered for **4-TEB**, although **2-TEB** has only one possible

distance between the S atoms.

Figure S3. DFT optimized structures of (a) **4-TEB** and (b) **2-TEB** with the various distances between the sulfur atoms of the thiol groups.



The length of the last plateau was defined as the distance between points (set points) at which the conductance dropped below $6.7 \times 10^{-5}G_0$ and $3.2 \times 10^{-5}G_0$ for **2-TEB**. The set points, which were determined from the conductance values and the standard deviation of the conductance values of the corresponding single-molecule junction, were $3.5 \times 10^{-4}G_0$ and $1.9 \times 10^{-4}G_0$ for **4-TEB**. The average lengths of the last plateau were 0.24 and 0.04 nm for the **4-TEB** and **2-TEB** molecular junctions, respectively. The longer last plateau of the **4-TEB** molecule junction indicated the higher stability. If the **4-TEB** molecule binds to the Au electrodes via two anchoring units, the length of the last plateau for the **4-TEB** molecule junction should be identical to that for the **2-TEB** molecule junction. The longer last plateau thus indicates that the **4-TEB** molecule actually binds to the Au electrodes via all four anchoring units.

The break distance is defined as the distance between points (set points) at which the conductance drops below $0.02G_0$ and $3.2 \times 10^{-5}G_0$ for **2-TEB**. The set points were $0.02G_0$ and $1.9 \times 10^{-4}G_0$ for **4-TEB**. When molecules do not bridge the nanogap electrodes, the conductance through

the nanogap exponentially decreases with the gap distance (d) according to the equation $G = A\exp(-\beta d)$, where the attenuation factor β is $\sim 2.0 \text{ \AA}^{-1}$.¹ The gap lengths (L_0) were determined to be 0.32 nm and 0.23 nm for **2-TEB** and **4-TEB** solutions, respectively, using the present set point values where the molecules did not bridge the nanogap. The peak around 0.2 nm for the **2-TEB** single-molecule junction (Figure 2a) corresponds to the L_0 where molecules do not bridge the nanogap. The appearance of the peak in the range of 0.2–0.3 nm for **2-TEB** indicates that there is a low formation probability (59%) for the molecular junctions, whereas the absence of a peak for **4-TEB** indicates that there is a high formation probability (99%) for the molecular junctions. When the molecule bridges the nanogap just after breaking the metal contact, the gap length should be longer than L_0 . Therefore, we evaluated the formation probability from the ratio of the number of the junctions whose break distance was larger than L_0 to the total number of junctions.

Just after breaking the Au atomic contact, a nanogap with a finite size formed due to the elastic response of the banks of the electrodes.^{S3,S4} The gap size was typically 0.4 nm for the Au atomic contact. The distance between metal electrodes in the molecular junction is the sum of the initial gap (L_i) of 0.4 nm and the break distance (L_b). The average L_b values were 0.37 nm and 0.94 nm for the **2-TEB** and **4-TEB** molecular junctions, respectively. Thus, the average distances between metal electrodes ($L_b + L_i$) were 0.8 and 1.3 nm for the **2-TEB** and **4-TEB** molecular junctions, respectively. During the junction stretching, the single-molecule junction can break before the molecule bridges in the fully stretched configuration. The maximum $L_b + L_i$ value rather than average $L_b + L_i$ value should be closer to the true size of the molecule bridging the electrodes. The maximum L_b values were 1.2 nm and 1.9 nm for the **2-TEB** and **4-TEB** molecular junctions, which meant that the maximum $L_b + L_i$ values were 1.6 nm and 2.3 nm, respectively.

Since Au-S distance was 0.24 nm for the **4-TEB** molecular junction (determined by present theoretical calculation), the Au-Au distance was expected to be 2.2 nm ($1.76 \text{ nm} + 2 \times 0.24 \text{ nm}$) for the **4-TEB** molecular junction, when the **4-TEB** molecule bridged between Au electrodes with its molecular longer axis was parallel to the junction axis. The close agreement between 2.3 nm obtained by gap length analysis and 2.2 nm obtained by analysis of the molecular size, supported the

structural model calculated in this study (Figure 4a). The Au-Au distance was expected to be 2.0 nm ($1.55 \text{ nm} + 2 \times 0.22 \text{ nm}$) for the **2-TEB** molecular junction using the calculated tilt angle of 35° with respect to junction axis and Au-S distance of 0.22 nm. Here again, the agreement between 1.6 nm obtained by gap length analysis and 2.0 nm obtained by analysis of the molecular size, supported the structural model calculated in this study (Figure 4c).

3. Fabrication of planar nanogap electrodes

Planar nanogap electrodes were fabricated using SiO_2 (300 nm)/Si wafers. These wafers were patterned by using conventional photolithography. After the first patterning process, the first metal layer (2 nm Cr and 30 nm Au) was deposited at 75° with respect to the substrate surface. The second lithography process was performed, and the second metal layer (2 nm Cr and 15 nm Au) was deposited at an angle of 60° to the opposite side of the first layer. Most of the electrodes had a random gap size and short circuits. The gap size of the nanogap electrodes was controlled to be around 1 nm by using an electromigration technique. Details for the fabrication of the nanogap electrodes are given in our previous report.²⁰ The gap size was evaluated to be 1 nm by fitting the I - V characteristics of the nanogap electrodes before the immersion process using Simmons' equation.⁵⁵

4. I - V and G - V curves of the 4-TEB junction

Figure S4 shows examples of the current-voltage characteristics (I - V curves) of the nanogap electrodes before and after the immersion process. The current increased after the immersion process, indicating the formation of a molecule bridge. The inset values are the numbers of molecules bridging the Au electrodes evaluated by comparing the conductance of the molecular junction with that of the single-molecule conductance. Figure S5 shows examples of the differential conductance curves (G - V curves) of nanogap electrodes after the immersion process. Peaks were observed around ± 0.8 V.

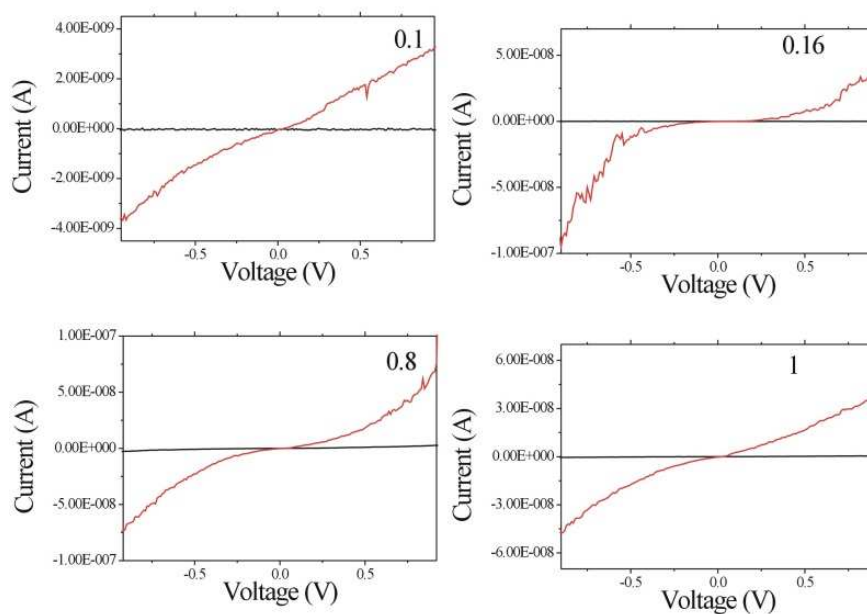


Figure S4. Examples of current–voltage characteristics before (black) and after (red) the immersion process. The inset is the number of molecules bridging Au electrodes, evaluated by comparing the conductance of the molecular junction with that of the single-molecule conductance.

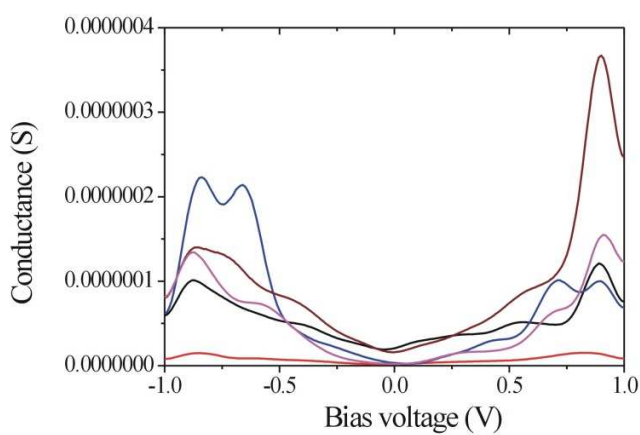


Figure S5. Differential conductance curves of nanogap electrodes after the immersion process.

S5: Calculated transmission coefficient

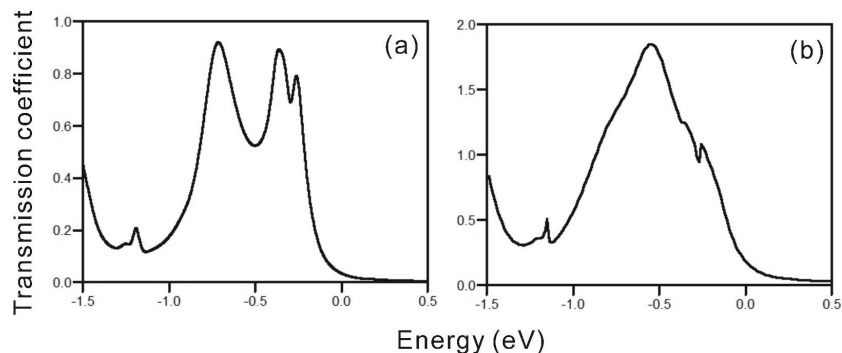


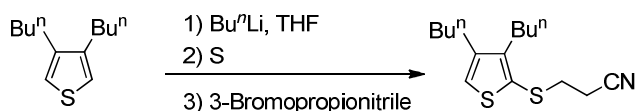
Figure S6. Calculated transmission coefficient for (a) **2ANC** and (b) **4ANC**.

S6. Synthesis of 4Ac-TEB and 2Ac-TEB

General methods

NMR spectra were recorded on a Bruker AV500 or a JEOL JNM-PMX 500 spectrometer using tetramethylsilane as an internal standard. Mass spectra were recorded on a SHIMADZU GCMS-QP2020 for the EI method or an AXIMA-CFR spectrometer for the LDI-TOF method. Elemental analyses were performed at the microanalysis laboratory of Tokyo Metropolitan University. Column chromatography was carried out using Daiso silica gel 1001W. All reactions were carried out under a nitrogen atmosphere. THF was freshly distilled from sodium benzophenone ketyl before use, and other solvents were purified using standard methods.

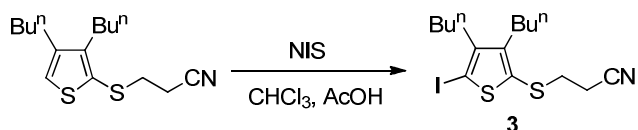
3,4-Dibutyl-2-(2-cyanoethylthio)thiophene



To a solution of 3,4-dibutylthiophene^{S6} (5.00 g, 25.5 mmol) in THF (50 mL) was added dropwise 1.65 M *n*-BuLi in hexane (16.2 mL, 26.8 mmol) via a syringe over 10 min at 0 °C. After stirring for 1 h at the same temperature, the mixture was cooled to -78 °C. Elemental sulfur (870 mg, 26.8 mmol) was added, and the mixture was stirred for 30 min at -78 °C and for an additional 30 min at room temperature. The reaction mixture was cooled to 0 °C, and 3-bromopropionitrile (6.89 g, 51.4

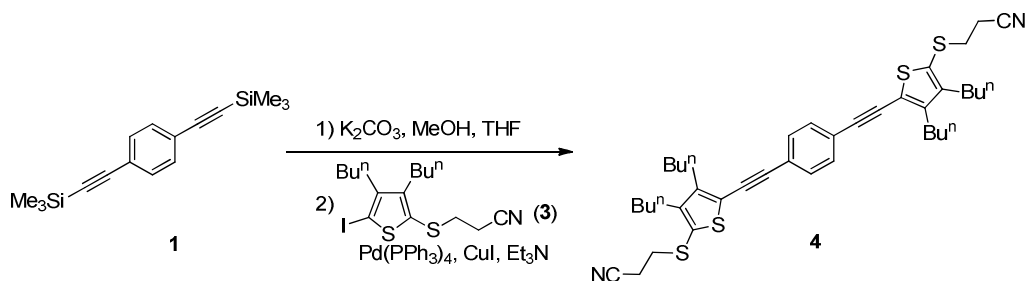
mmol) was added dropwise via a syringe. The resulting solution was stirred for 1 h at room temperature. After the slow addition of 2M HCl, the aqueous layer was extracted three times with CH₂Cl₂. The combined organic layer was dried over MgSO₄, and the solvent was removed by evaporation. The crude product was purified by using column chromatography on silica gel with hexane□CH₂Cl₂ (2:1, v/v) as the eluent to afford 3,4-dibutyl-2-(2-cyanoethylthio)thiophene as a pale yellow oil (6.55 g, 91%). ¹H NMR (CDCl₃, 500 MHz): δ = 7.01 (s, 1H), 2.92 (t, *J* = 7.5 Hz, 2H), 2.70–2.63 (m, 2H), 2.59 (t, *J* = 7.5 Hz, 2H), 2.54–2.48 (m, 2H), 1.65–1.57 (m, 2H), 1.48–1.34 (m, 6H), 0.96 (t, *J* = 7.5 Hz, 3H), 0.95 (t, *J* = 7.5 Hz, 3H). ¹³C NMR (CDCl₃, 125 MHz): δ = 148.31, 143.07, 124.98, 123.97, 118.07, 33.69, 32.93, 31.73, 29.21, 27.52, 22.84, 22.62, 18.14, 13.98, 13.94; EI-MS *m/z* 281 (M⁺); Anal. Calcd for C₁₈H₂₄S: C, 64.00%; H, 8.24%; N, 4.98%. Found: C, 64.25%; H, 8.27%; N, 4.75%.

3,4-Dibutyl-5-(2-cyanoethylthio)-2-iodothiophene (3)



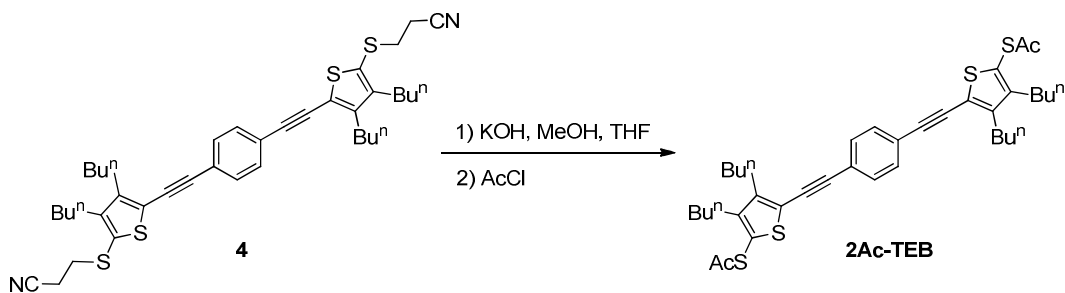
To a solution of 3,4-dibutyl-2-(2-cyanoethylthio)thiophene (4.14 g, 14.7 mmol) in CHCl₃ (160 mL) and AcOH (40 mL) was added portionwise *N*-iodosuccinimide (3.46 g, 15.4 mmol) at 0 °C. The reaction mixture was stirred for 14 h at room temperature. After addition of sat. aq. NaHCO₃ solution, the aqueous layer was extracted three times with CH₂Cl₂. The combined organic layer was dried over MgSO₄, and the solvent was removed by evaporation. The crude product was purified by column chromatography on silica gel with hexane□CH₂Cl₂ (2:1, v/v) as the eluent to afford **3** as a yellow viscous oil (4.90 g, 82%). **3**: ¹H NMR (CDCl₃, 500 MHz): δ = 2.92 (t, *J* = 7.3 Hz, 2H), 2.73–2.67 (m, 2H), 2.60 (t, *J* = 7.3 Hz, 2H), 2.54–2.48 (m, 2H), 1.50–1.34 (m, 8H), 0.97 (t, *J* = 7.3 Hz, 3H), 0.95 (t, *J* = 7.5 Hz, 3H). ¹³C NMR (CDCl₃, 125 MHz): δ = 148.33, 147.20, 129.90, 117.84, 78.54, 33.75, 33.30, 31.96, 31.35, 28.21, 22.81, 22.78, 18.24, 13.89, 13.87. EI-MS *m/z* 407 (M⁺). Anal. Calcd for C₁₅H₂₃NS₂: C, 44.22%; H, 5.44%; N, 3.44%. Found: C, 44.16%; H, 5.35%; N, 3.37%.

1,4-Bis(3,4-dibutyl-5-(2-cyanoethylthio)-2-thienylethynyl)benzene (**4**)



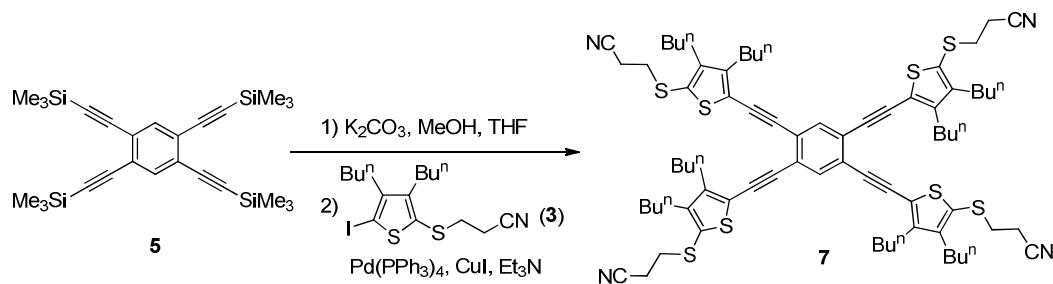
A mixture of 1,4-bis(trimethylsilylethynyl)benzene (**1**, 549 mg, 2.03 mmol) and K₂CO₃ (796 mg, 5.76 mmol) in THF (50 mL) and MeOH (50 mL) was stirred for 30 min at room temperature. After dilution with Et₂O (60 mL), the organic layer was washed three times with H₂O. The organic layer was dried over MgSO₄, and the solution was concentrated by using a rotary evaporator until the volume was ~15 mL. To the solution of 1,4-diethynylbenzene **2** was added a solution of 3,4-dibutyl-5-(2-cyanoethylthio)-2-iodothiophene (**3**, 2.366 g, 5.80 mmol), Pd(PPh₃)₄ (116 mg, 0.10 mmol), CuI (65 mg, 0.34 mmol) in THF (40 mL), and diisopropylamine (DIPA, 4 mL), and the mixture was stirred for 14 h at room temperature. After addition of sat. NH₄Cl aq, the aqueous layer was extracted three times with CH₂Cl₂. The combined organic layer was dried over MgSO₄, and the solvent was evaporated. The crude product was purified by using column chromatography on silica gel with a mixed solvent (hexane/CH₂Cl₂ = 1:1, v/v) as the eluent to afford **4** as a pale yellow solid (1.31 g, 94%). **4**: ¹H NMR (CDCl₃, 500 MHz): δ = 7.45 (s, 4 H), 2.98 (t, *J* = 7.2 Hz, 4H), 2.72–2.62 (m, 12H), 1.62–1.59 (m, 4H), 1.47–1.40 (m, 12H), 0.99–0.95 (m, 12H). ¹³C NMR (CDCl₃, 125 MHz): δ = 148.03, 147.98, 131.21, 126.82, 122.94, 121.64, 117.82, 96.26, 84.21, 33.58, 33.14, 32.40, 28.81, 27.82, 22.81, 22.78, 18.26, 13.96, 13.91. EI-MS *m/z* 684 (M⁺). Anal. Calcd for C₄₀H₄₈N₂S₄: C, 70.13%; H, 7.06%; N, 4.09%. Found: C, 70.13%; H, 7.04%; N, 4.06%.

1,4-Bis(3,4-dibutyl-5-acetylthio-2-thienylethynyl)benzene (2Ac-TEB)



To a solution of 1,2-bis(3,4-dibutyl-5-(2-cyanoethylthio)-2-thienylethynyl)benzene (**4**, 144 mg, 0.211 mmol) in THF (30 mL) was slowly added a solution of KOH (50 mg, 0.89 mmol) in methanol (3.5 mL) at 0 °C and stirred for 20 min at the same temperature. The mixture was cooled to -78 °C, and a solution of acetyl chloride (66 mg, 0.84 mmol) in THF (5 mL) was added. The resulting mixture was stirred for 1 h at room temperature. The reaction was quenched by adding H₂O, and the aqueous layer was extracted three times with CH₂Cl₂. The organic layer was washed with brine and dried over MgSO₄. The solvent was evaporated, and the crude product was purified by using column chromatography on silica gel with hexane□CH₂Cl₂ (1:1, v/v) as the eluent to afford **2Ac-TEB** as a yellow solid (125 mg, 90%). **2Ac-TEB**: ¹H NMR (CDCl₃, 500 MHz): δ = 7.45 (s, 4H), 2.72 (t, J = 7.8 Hz, 4H), 2.53 (t, J = 7.6 Hz, 4H), 2.41 (s, 6H), 1.65–1.59 (m, 4H), 1.47–1.34 (m, 12H), 0.99–0.92 (m, 12H). ¹³C NMR (CDCl₃, 125 MHz): δ = 194.16, 148.18, 147.55, 131.18, 123.48, 122.96, 120.81, 96.60, 84.27, 32.46, 32.37, 29.60, 28.74, 27.81, 22.74, 22.72, 13.94, 13.84. EI-MS m/z 662 (M⁺). Anal. Calcd for C₃₈H₄₆O₂S₄: C, 68.84%; H, 6.99%. Found: C, 68.88%; H, 6.99%.

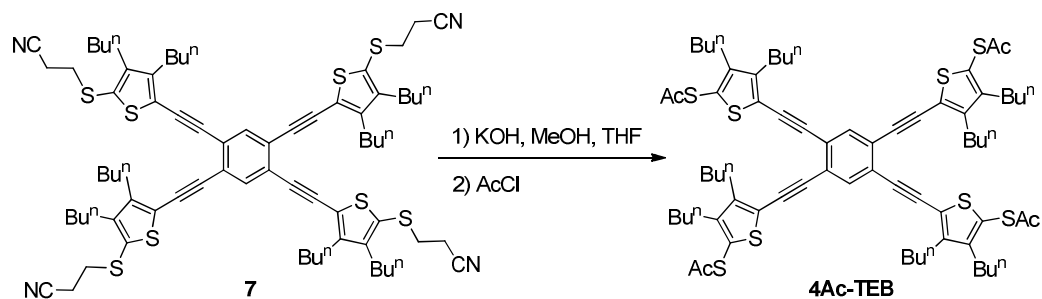
1,2,4,5-Tetrakis(3,4-dibutyl-5-(2-cyanoethylthio)-2-thienylethynyl)benzene (**7**)



A mixture of 1,2,4,5-tetrakis(trimethylsilyl)ethynylbenzene (**5**, 305 mg, 0.66 mmol) and K₂CO₃

(124 mg, 0.897 mmol) in THF (10 mL) and MeOH (10 mL) was stirred for 30 min at room temperature. After dilution with Et₂O (60 mL), the organic layer was washed three times with H₂O. The organic layer was dried over MgSO₄, and the solution was concentrated by using a rotary evaporator until the volume was ~15 mL. The solution was added to a mixture of 3,4-dibutyl-5-(2-cyanoethylthio)-2-iodothiophene (**3**, 1.634 g, 4.01 mmol), Pd(PPh₃)₄ (79 mg, 0.068 mmol), CuI (66.7 mg, 0.35 mmol) in THF (20 mL), and triethylamine (5 mL), and the resulting mixture was stirred for 14 h at room temperature. After addition of sat. aq. NH₄Cl solution, the aqueous layer was extracted three times with CH₂Cl₂. The combined organic layer was dried over MgSO₄, and the solvent was evaporated. The crude product was purified by using column chromatography on silica gel with CH₂Cl₂ as eluent to afford **7** (540 mg, 63%). **7**: ¹H NMR (CDCl₃, 500 MHz): δ = 7.61 (s, 2H), 3.00 (t, *J* = 7.5 Hz, 8H), 2.73–2.64 (m, 24H), 1.59–1.56 (m, 8H), 1.43–1.34 (m, 24H), 0.98–0.90 (m, 24H). ¹³C NMR (CDCl₃, 125 MHz): δ = 148.60, 147.99, 134.60, 127.72, 124.55, 121.21, 117.80, 94.35, 88.38, 33.59, 33.12, 32.45, 28.96, 27.78, 22.79, 22.66, 18.25, 13.93, 13.90. LDI-TOF-MS *m/z* Calcd for C₇₄H₉₀N₄S₈: 1290.49, Found: 1290.77. Anal. Calcd for C₇₄H₉₀N₄S₈: C, 68.79%; H, 7.02%; N, 4.34%. Found: C, 68.80%; H, 6.88%; N, 4.45%.

1,2,4,5-Tetrakis(3,4-dibutyl-5-acetylthio-2-thienylethynyl)benzene (4Ac-TEB)



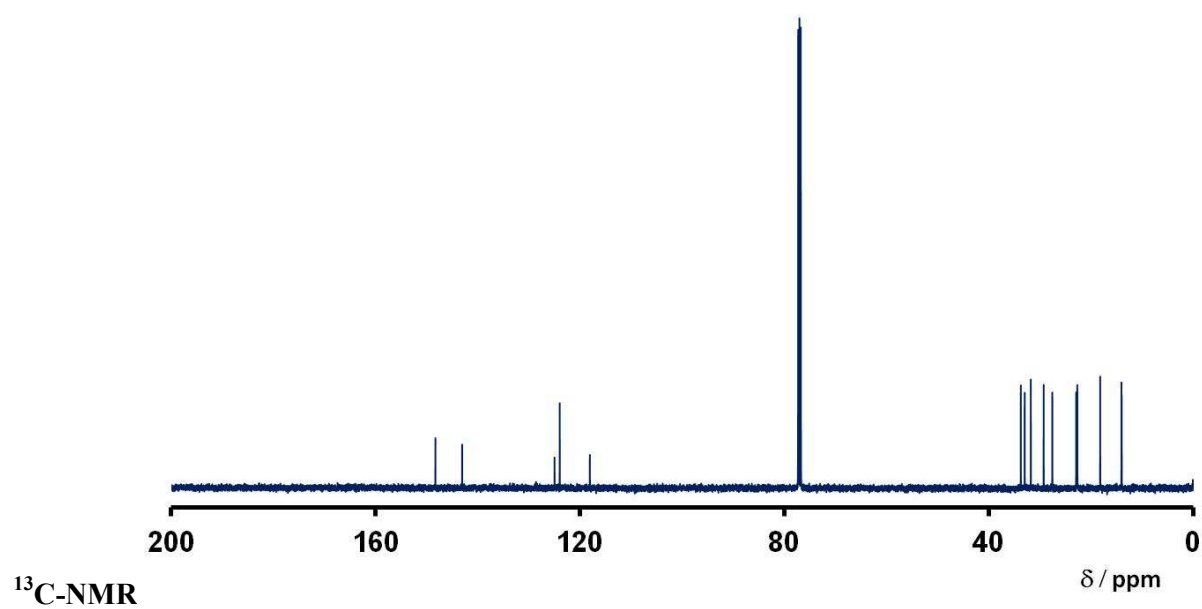
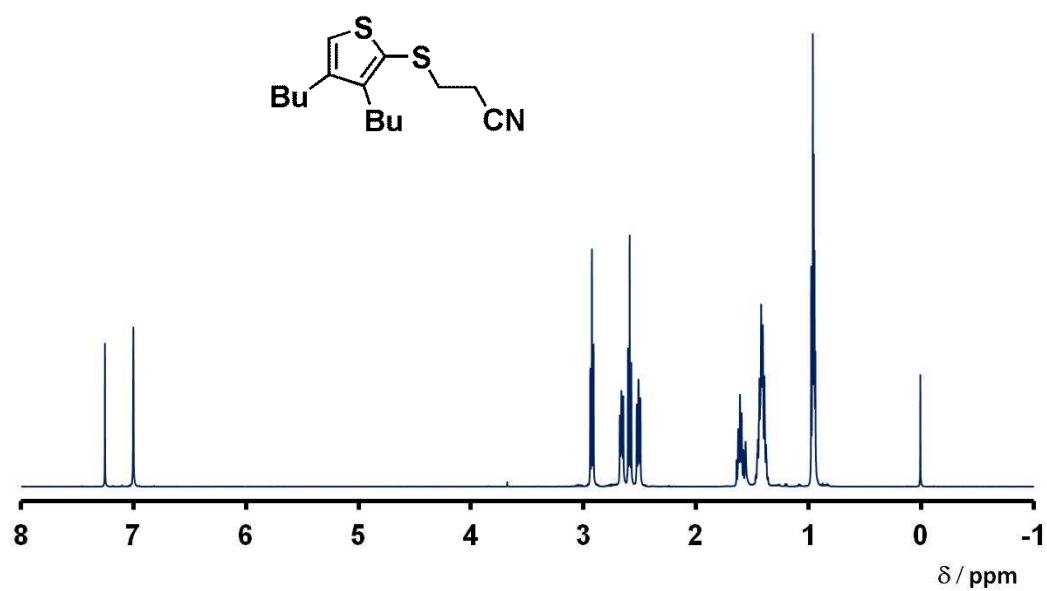
To a solution of 1,2,4,5-tetrakis(3,4-dibutyl-5-(2-cyanoethylthio)-2-thienylethynyl)benzene (**7**, 308 mg, 0.24 mmol) in THF (30 mL) was added slowly a solution of KOH (76.9 mg, 1.37 mmol) in methanol (3.5 mL) at 0 °C, and the solution was stirred for 20 min at the same temperature. A solution of acetyl chloride (154.5 mg, 1.97 mmol) in THF (10 mL) was added at 0 °C, and the

mixture stirred for 1 h at room temperature. The reaction was quenched by adding H₂O, and the aqueous layer was extracted three times with CH₂Cl₂. The organic layer was washed with brine. The organic layer was dried over MgSO₄, and the solvent was evaporated. The crude product was purified by using column chromatography on silica gel with hexane-CH₂Cl₂ (1:1, v/v) as the eluent and recrystallized from CH₂Cl₂ and methanol to afford **4Ac-TEB** as feather-like bright yellow crystals (107 mg, 36%). **4Ac-TEB**: ¹H NMR (CDCl₃, 500 MHz): δ = 7.63 (s, 2H), 2.74 (t, *J* = 7.5 Hz, 8H), 2.54 (t, *J* = 7.5 Hz, 8H), 2.41 (s, 12H), 1.58–1.54 (m, 8H), 1.44–1.33 (m, 24H), 0.94–0.88 (m, 24H). ¹³C NMR (CDCl₃, 125 MHz): δ = 194.08, 148.33, 148.18, 134.89, 124.59, 123.12, 121.69, 94.68, 88.42, 32.45(2C), 29.58, 28.93, 27.79, 22.72, 22.60, 13.94, 13.84. LDI-TOF-MS *m/z* Calcd for C₇₀H₈₆O₄S₈: 1246.43. Found: 1246.23. Anal. Calcd for C₇₀H₈₆O₄S₈: C, 67.37%; H, 6.95%. Found: C, 67.06%; H, 6.98%.

S5. NMR spectra

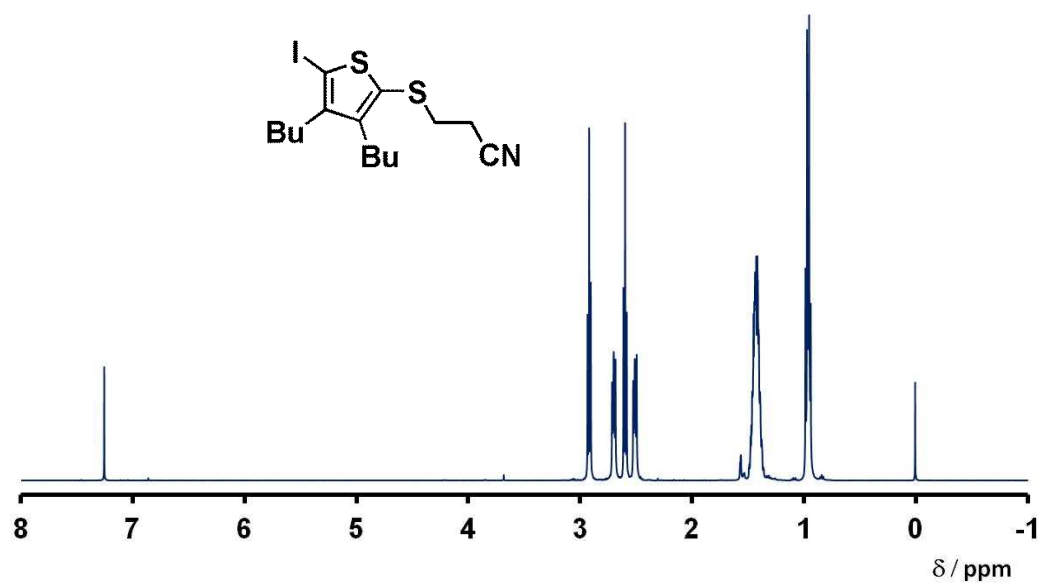
3,4-Dibutyl-2-(2-cyanoethylthio)thiophene

$^1\text{H-NMR}$

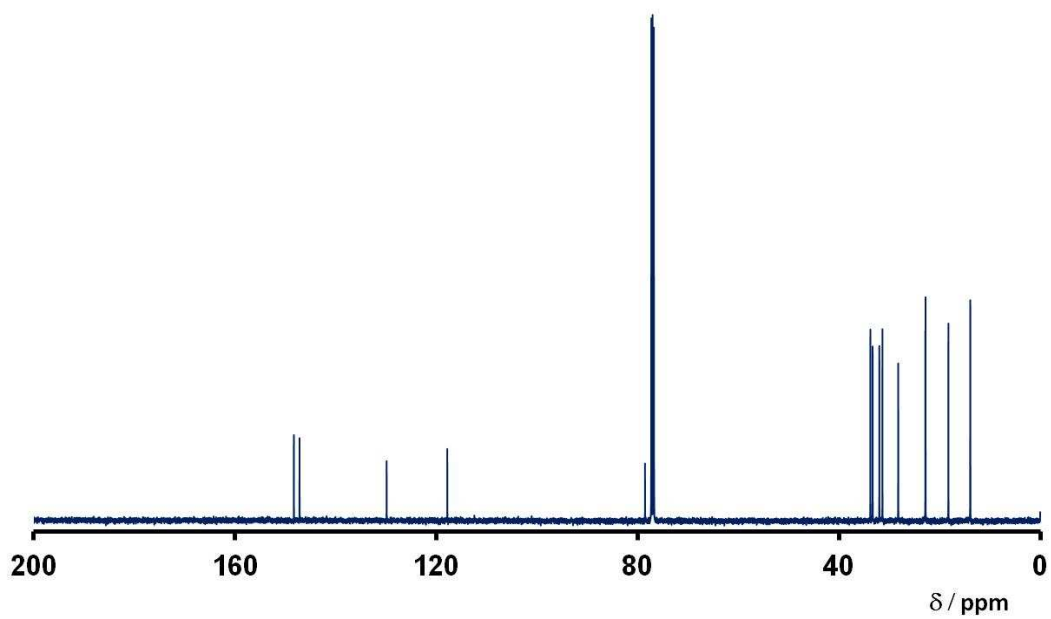


3,4-Dibutyl-5-(2-cyanoethylthio)-2-iodothiophene (3)

¹H-NMR

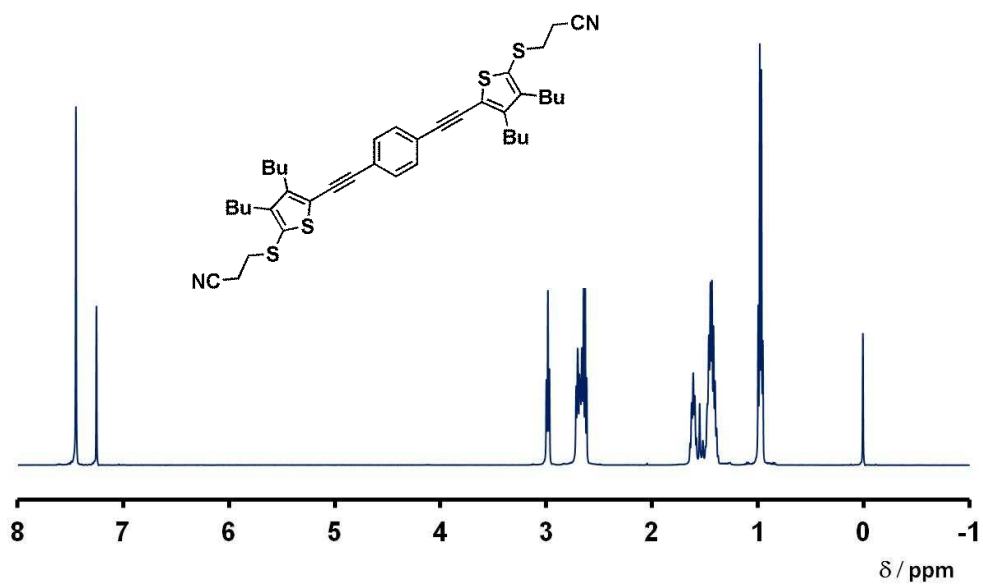


¹³C-NMR

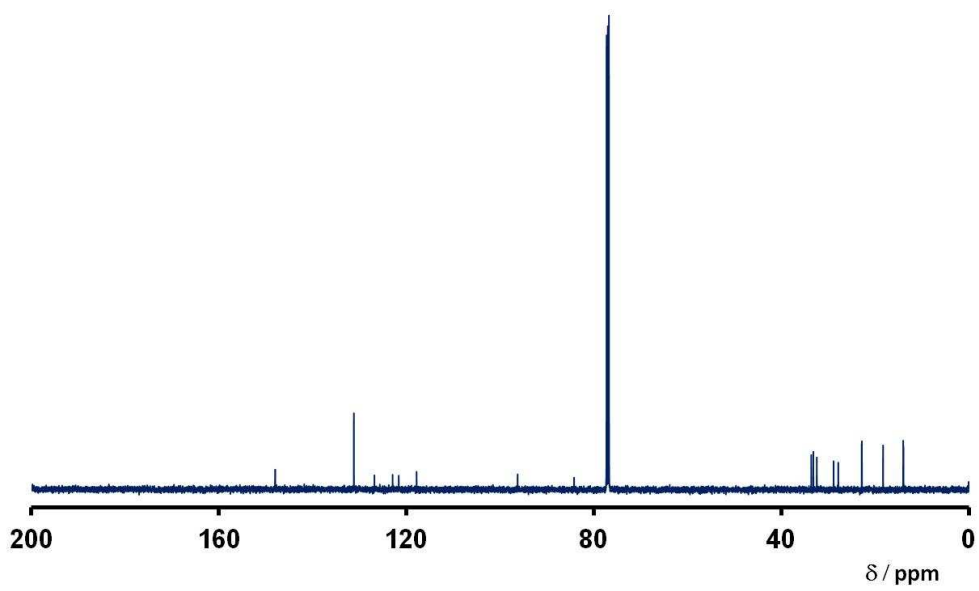


1,4-Bis(3,4-dibutyl-5-(2-cyanoethylthio)-2-thienylethynyl)benzene (4)

¹H-NMR

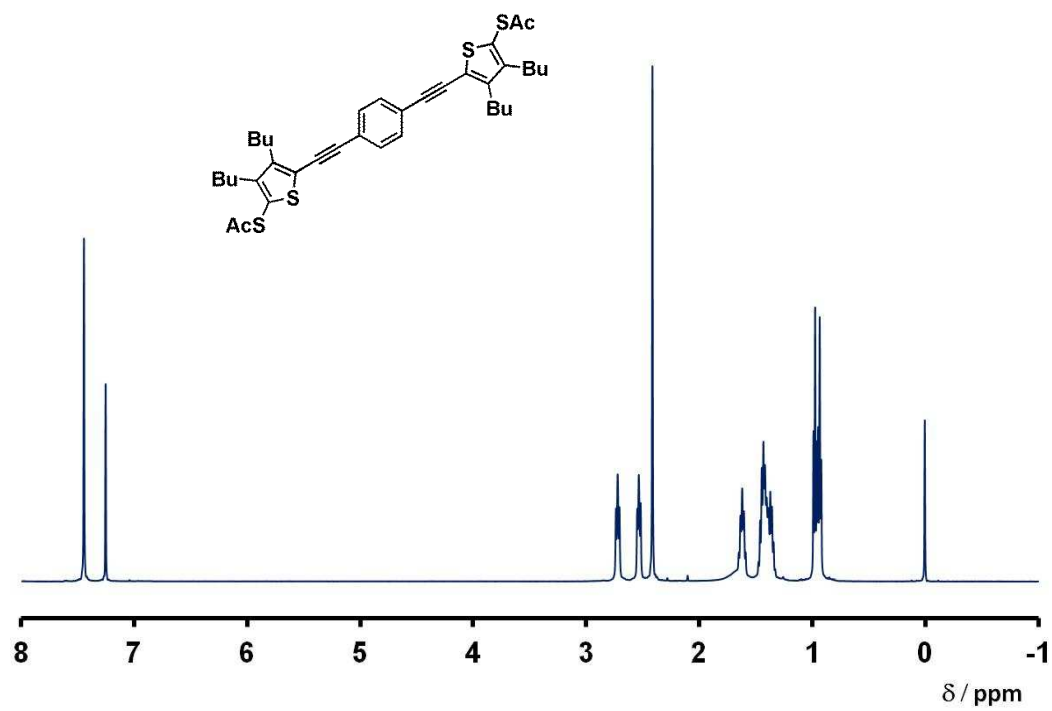


¹³C-NMR

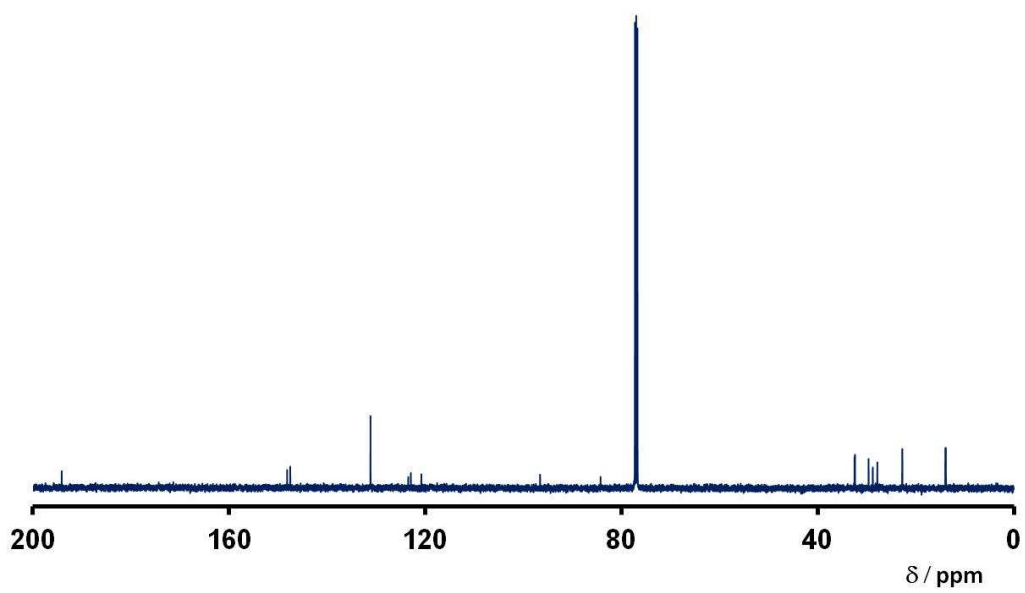


1,4-Bis(3,4-dibutyl-5-acetylthio-2-thienylethynyl)benzene (2Ac-TEB)

¹H-NMR

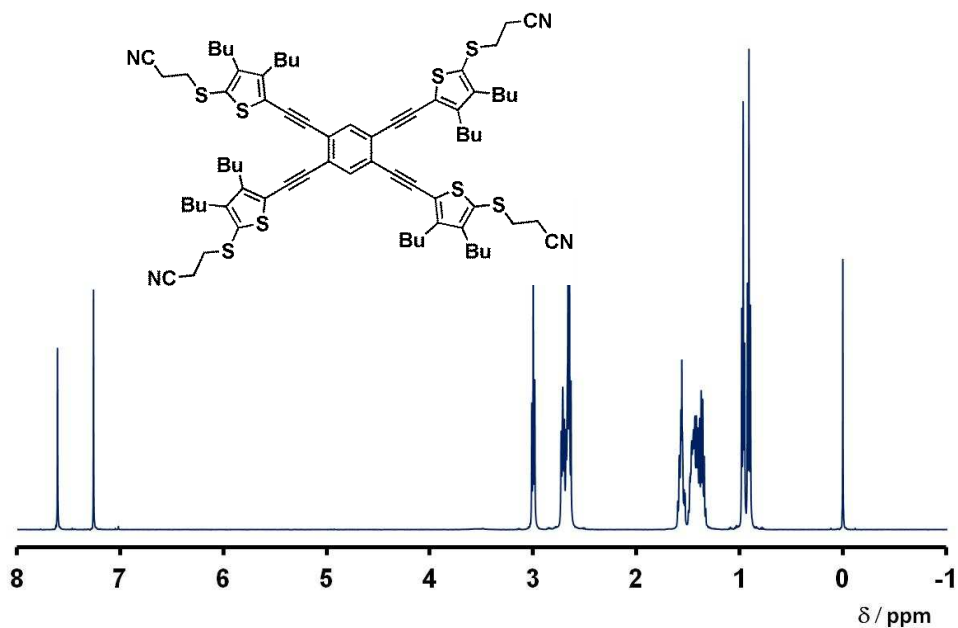


¹³C-NMR

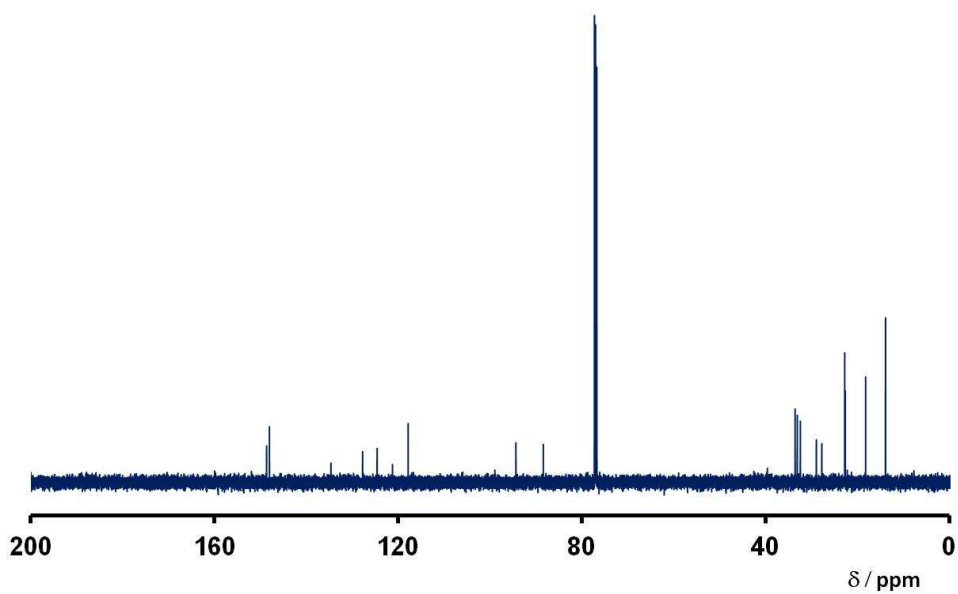


1,2,4,5-Tetrakis(3,4-dibutyl-5-(2-cyanoethylthio)-2-thienylethynyl)benzene (7)

¹H-NMR

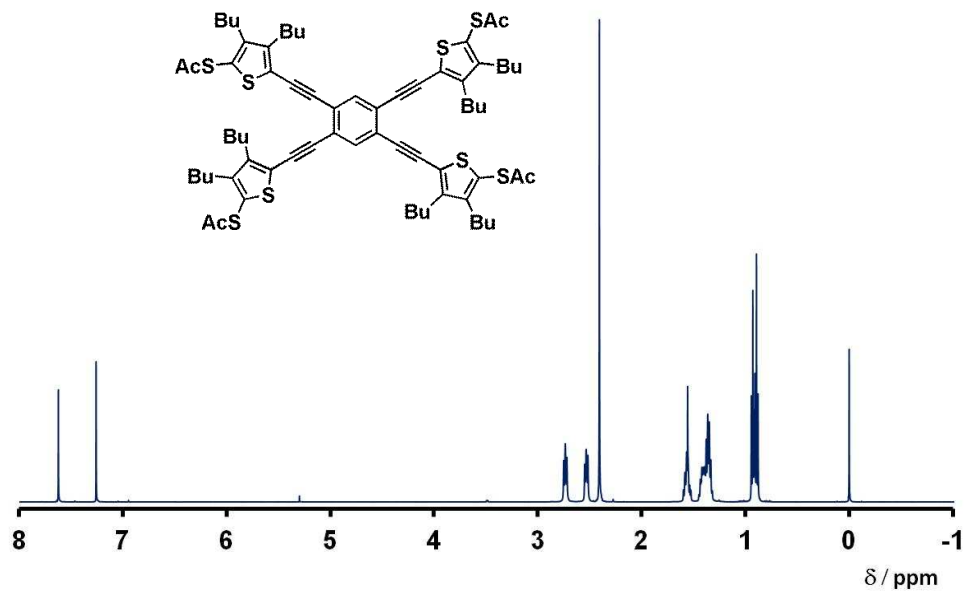


¹³C-NMR

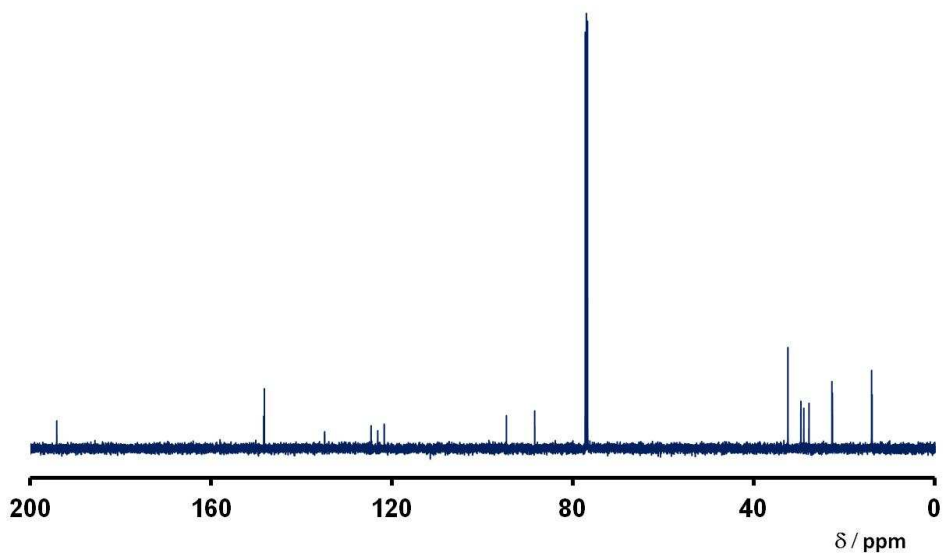


1,2,4,5-Tetrakis(3,4-dibutyl-5-acetylthio-2-thienylethynyl)benzene (4Ac-TEB)

¹H-NMR



$^{13}\text{C-NMR}$



References

- S1) Huber, R.; Gonzalez, M. T.; Wu, S.; Langer, M.; Grunder, S.; Horhoiu, V.; Mayor, M.; Bryce, M. R.; Wang, C.; Jitchati, R.; Schonenberger, C.; Calame, M. Electrical Conductance of Conjugated Oligomers at the Single Molecule Level. *J. Am. Chem. Soc.* **2008**, *130*, 1080-1084.
- S2) Martin, C. A.; Ding, D.; Sorensen, J. K.; Bjornholm, T.; van Ruitenbeek, J. M.; van der Zant, H. S. J. Fullerene-Based Anchoring Groups for Molecular Electronics. *J. Am. Chem. Soc.* **2008**, *130*, 13198–13199.
- S3) Tsutsui, M.; Ohshiro, T.; Matsubara, K.; Furuhashi, M.; Taniguchi, M.; Kawai, T. Atomically Controlled Fabrications of Subnanometer Scale Electrode Gaps. *J. Appl. Phys.* **2010**, *108*, 064312.
- S4) Zhao, J.; Murakoshi, K.; Yin, X.; Kiguchi, M.; Guo, Y.; Wang, N.; Liang, S.; Liu, H. Dynamic Characterization of the Postbreaking Behavior of a Nanowire. *J. Phys. Chem. C* **2008**, *112*, 20088–20094.
- S5) Naitoh, Y.; Liang, T.-T.; Azebara, H. Mizutani, W. Measuring Molecular Conductivities Using Single Molecular-Sized Gap Junctions Fabricated without Using Electron Beam Lithography. *Jpn. J. Appl. Phys.* **2005**, *44*, L472.
- S6) Tamao, K.; Kodama, S.; Nakajima, I.; Kumada, M.; Minato, A.; Suzuki, K. Nickel-Phosphine Complex-Catalyzed Grignard Coupling—II : Grignard Coupling of Heterocyclic Compounds. *Tetrahedron* **1982**, *38*, 3347.